Journal of Power Sources 182 (2008) 188–196

Contents lists available at ScienceDirect

Journal of Power Sources

journal homepage: www.elsevier.com/locate/jpowsour

Synthesis and properties of a barium aluminosilicate solid oxide fuel cell glass–ceramic sealant

K.D. Meinhardt, D.-S. Kim, Y.-S. Chou, K.S. Weil*

Pacific Northwest National Laboratory, Richland, WA 99352, United States

ARTICLE INFO

Article history:
Received 15 February 2008
Received in revised form 19 March 2008
Accepted 20 March 2008
Available online 7 April 2008

Keywords:
Solid oxide fuel cell (SOFC)
Glass–ceramic sealant
Coefficient of thermal expansion

ABSTRACT

A series of barium aluminosilicate glasses modified with CaO and B_2O_3 were prepared and evaluated with respect to their suitability in sealing planar solid oxide fuel cells (SOFCs). At a target operating temperature of 750 °C, the long-term coefficient of thermal expansion (CTE) of one particular composition (35 mol% BaO, 15 mol% CaO, 10 mol% B_2O_3, 5 mol% Al_2O_3, and bal. SiO_2) was found to be particularly stable, due to devitrification to a mixture of glass and ceramic phases. This sealant composition exhibits minimal chemical interaction with the yttria-stabilized zirconia electrolyte, yet forms a strong bond with this material. Interactions with metal components were found to be more extensive and depended on the composition of the metal oxide scale that formed during sealing. Generally alumina-scale formers exhibited a more compact reaction zone with the glass than chromia-scale forming alloys. Mechanical measurements conducted on the bulk glass–ceramic and on seals formed using these materials indicate that the sealant is anticipated to display adequate long-term strength for most conventional stationary SOFC applications.

1. Introduction

The operation and performance of a solid oxide fuel cell (SOFC) stack is partially dependent on having robust gas-tight seals that prevent the mixing of the fuel and oxidizer gas streams [1,2]. The presence of leaks, due to flaws formed during stack manufacture or as a result of component degradation during stack operation, lead to reduced system performance, lower power generation efficiency, and poor fuel utilization [3,4]. They can also cause local hot spots or worse, widespread internal combustion in the stack, both of which induce accelerated degradation in the device [4]. In a planar stack design this means that the central core of the cell, i.e., the ceramic electrolyte layer, must be dense and connected to the rest of the device with a high temperature, gas-tight seal. To date, one of the limiting challenges in fabricating planar SOFCs is how to properly join the ceramic cell to the metallic body of the device and ensure that a long-term, hermetic seal is formed. Typical conditions under which these devices are expected to operate and to which the accompanying seals will be exposed include: (1) an average operating temperature of 750 °C; (2) continuous exposure to an oxidizing atmosphere on the cathode side and a wet reducing gas on the anode side; and (3) anticipated lifetimes in the tens of thousands of hours.

Among the first and still most important sealants employed by pSOFC stack builders are high-temperature glasses and glass–ceramics [5,6]. This is because these materials:

- tend to display acceptable stability in the reducing and oxidizing atmospheres of the stack;
- are generally inexpensive;
- can be readily applied to the sealing surfaces as a powder dispersed in a paste or a tape cast sheet;
- typically exhibit good wetting behavior on both sealing surfaces (generally yttria-stabilized zirconia (YSZ) and stainless steel);
- are electrically insulating;
- can be engineered to exhibit a coefficient of thermal expansion (CTE) matching those of the adjacent pSOFC components in the final joint, thereby mitigating the generation of thermally induced stresses.

Many glass seal formulations are designed to soften and flow at a temperature above that required for stack operation in order to form a hermetic seal, predominantly via chemical bonding with the adjoining substrates. During the sealing operation, the glass partially or fully crystallizes to form a rigid, bonded seal. Crystallization is advantageous because the resulting material is typically

* Corresponding author. Tel.: +1 509 375 6796; fax: +1 509 375 4448.
E-mail address: Scott.Weil@pnl.gov (K.S. Weil).

0378-7753/$ – see front matter © 2008 Elsevier B.V. All rights reserved.
doi:10.1016/j.jpowsour.2008.03.079

stronger than the starting glass. However because the final joint is brittle, it is susceptible to fracture when exposed to tensile stresses of the type encountered during non-equilibrium thermal events or due to thermal expansion mismatches between the sealant and adjacent substrates [7,8]. Therefore, the sealant must be tailored to match the coefficients of thermal expansion of the adjacent substrates, which in turn must be selected to closely match each other [9]. Even a modest degree of thermal expansion mismatch can cause measurable bowing in the cells, which can subsequently lead to fuel and air maldistribution in the stack and result in reduced stack performance [10]. For these reasons, the metal stack components are typically fabricated from ferritic stainless steel (CTE of $12–13 \times 10^{-6}\,K^{-1}$) [11] to approximately match the composite CTE of the cell (CTE of $10.5–12.5 \times 10^{-6}\,K^{-1}$, depending on whether the cell is electrolyte- or anode-supported) [11]. Significant effort has been expended on developing sealing materials with CTEs in this range.

Phosphate, boron, and silica-based glasses and glass–ceramics have all been previously evaluated for use in sealing pSOFCs [12–17]. Work conducted by Larsen et al. [12] revealed a number of challenging problems with glasses based purely on phosphate as the glass former. At temperature, the phosphate volatilized and reacted with the Ni/yttria-stabilized zirconia-based anode to form nickel phosphide and zirconium oxyphosphate. Additionally, when de-vitrified these phosphate glasses typically form meta- or pyrophosphates, both of which exhibit low stability in humidified fuel gas at temperatures greater than 700 °C. Borosilicate glasses and glass ceramics have also been considered as potential pSOFC sealing materials. However, investigations conducted by Günther et al. [4] and by Ley et al. [5] indicate that the boron undergoes significant reaction with humidified hydrogen (the fuel used in SOFCs) to form several gaseous species including $B_2(OH)_2$ and $B_2(OH)_3$ at operating temperature. That is, any high boria-containing seal (approximately >10 mol% B_2O_3) will likely undergo measurable corrosion over time in a humidified fuel environment. Glasses with B_2O_3 as the only glass former display as much as a 20% weight loss in humidified hydrogen and also exhibit extensive interactions with stack component materials under both air and wet fuel gas atmospheres [13].

Silica-based glasses and glass–ceramics offer greater promise. They typically exhibit higher chemical resistance and little interaction with the stack components [18]. Unfortunately, these glasses tend to have thermal expansions below the range needed for a sealing material. To date, the best results have been obtained using compositions based on silica with various modifiers added to increase CTE and improve adhesion and joint strength. While alkali silicate glasses tend to interact deleteriously with the cell materials [19], the use of alkaline–earths to form systems such as $BaO–CaO–SiO_2$ [20] and $BaO–Al_2O_3–SiO_2$ [13] yield glass–ceramics with much higher chemical resistance and far less reactivity toward other stack components [21,22].

As suggested from the prior art and through feedback from stack developers, there are several challenges in developing an acceptable glass–ceramic for pSOFC sealing, the first of which is achieving the proper balance of material properties that results in a sealing process which is consistent and repeatable. The example shown in Fig. 1 illustrates the importance of controlling material viscosity as a function of temperature. The starting glass must be fluid enough at the temperature of sealing to wet the sealing surfaces, yet not so fluid that it flows out from between the substrates and results in open gaps and subsequent leaks. By control ling the kinetics of crystallization, it is possible to slowly raise the viscosity of the sealant so that it attains the proper stiffness after wetting to minimize excessive flow or "squeeze out". In addition to viscosity, there

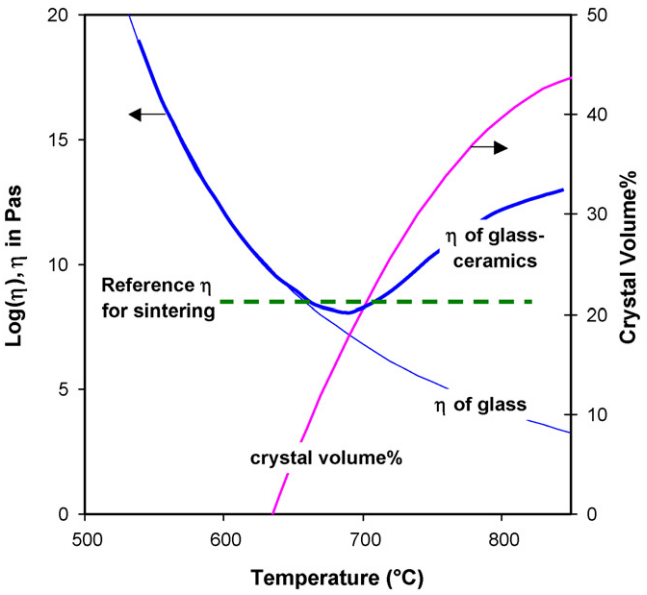

Fig. 1. A schematic of the type of viscosity ("greek symbol eta") and degree of crystallization behavior as a function of temperature seen in many sealing glasses. Note that the viscosity curve for the glass–ceramic exhibits a minimum as a result of the intersection between the crystallization and extrapolated glass viscosity curves.

are several other key material parameters that must be simultaneously controlled to achieve a robust sealing process, including: T_g, T_s (the temperature at which the glass first softens), time dependent CTE, wetting behavior, and bulk strength. The glass–ceramic sealant discussed in detail below (referred to as G-18) has been employed in fabricating a number of large-scale developmental stacks that have been operated for upwards of 4600 h [23]. While the sealant has been referenced in a number of publications, its synthesis and properties are described explicitly for the first time here.

2. Experimental

2.1. Materials

The barium aluminosilicate system (BAS, $BaO–Al_2O_3–SiO_2$) was chosen as the starting point for glass composition development because of its potential for good glass-forming properties, the well-studied/well-understood phase equilibria in this system, and its high coefficients of thermal expansion. The alumina content has a strong influence on the rate of crystallization in the glass, and therefore its viscosity, during heat treatment. In addition, the use of a small amount of boron oxide (B_2O_3, a lower-temperature glass former) was explored as a combination viscosity modifier/wetting agent and La_2O_3 was investigated as a viscosity modifier and long-term CTE stabilizer. Listed in Table 1 are a series of these and other compositional modifiers that are commonly added to alter the initial bulk properties of the glass–ceramic [24].

All of the glass formulations were prepared by melting the thoroughly blended constituent compounds in a platinum crucible under static air conditions at 1300 °C for 3 h. The constituents, $Ba(CO_3)_2$ and $Ca(CO_3)_2$ (both of which convert to their respective oxides during glass formation), Al_2O_3, B_2O_3, La_2O_3, and SiO_2, were obtained from Aldrich Chemical Company in reagent grade. Once melted and quenched, each batch of glass was ball milled to an average particle diameter (D_{50}) of 22 μm. As a powder, the glass could be compacted to form pellets and bars for wetting, adhesion, and mechanical testing or mixed with an organic binder system to form a paste that could be dispensed directly onto a substrate or

Table 1
Common compositional modifiers for silicate-based glass–ceramic sealants

Modifier	Function
Al_2O_3	Allows control over viscosity through the rate of crystallization
B_2O_3	Reduces CTE, T_g, T_s, and viscosity and improves wetting
BaO, CaO, MgO	Reduces T_g and T_s, and raises CTE in the glass–ceramic
Cr_2O_3, V_2O_5	Reduces surface tension
La_2O_3, Nd_2O_3, Y_2O_3,	Used as a viscosity modifier and long-term CTE stabilizer
CuO, NiO, CoO, MnO	Improves surface adherence
TiO_2, ZrO_2, SrO	Nucleates crystallization

slurry cast into tapes which could be laminated to the appropriate thickness and cut into shapes for use in joining.

Anode-supported bilayers, consisting of NiO/5YSZ (zirconia stabilized with 5 mol% yttria) as the anode and 8YSZ as the electrolyte, and thin gage stainless steel (FeCrAlY and 446, both ferritic alloys) were employed as model substrates in this study. Disc-shaped bilayer coupons were fabricated by traditional tape casting and co-sintering techniques and measured 25 mm in diameter by ~600 μm in thickness, with an average electrolyte thickness of ~8 μm. As-received 300 μm thick FeCrAlY and 446 sheets were cut into washer-shaped specimens (44 mm in diameter with a 15 mm diameter concentric hole) for joint strength testing. Glass pastes were prepared by mixing frit with Ferro 1573 binder in a volumetric ratio of 60:40. The paste was dispensed onto substrate surfaces (metal washers and YSZ side of the bilayer discs) at a uniform rate of 0.075 g/linear cm using an automated syringe dispenser. Each disc was then concentrically positioned on a washer specimen, loaded with a 50-g weight, and heated in air under the following sealing schedule: heat from room temperature to 850 °C at 10 °C min^{-1}, hold at 850 °C for 1 h, cool to 750 °C at 5 °C min^{-1}, hold at 750 °C for 4 h, and cool to room temperature at 5 °C min^{-1}.

2.2. Testing and characterization

Measurements of CTE as a function of temperature were conducted on 2.5 cm × 0.3 cm × 0.3 cm bars of bulk glass in the as-formed and as-aged conditions using a dilatometer (Unitherm Model 1161, Anter Corporation, Pittsburgh, PA). Room temperature X-ray diffraction (XRD) analysis of the nascent glasses and aged glass–ceramics was performed on powdered samples using a Philips Wide-Range Vertical Goniometer (Philips Ltd., Netherlands) and a Philips XRG3100 X-ray Generator over a scan range of 20–80° 2Θ with a 0.04° step size and 1 s hold time. XRD pattern analysis was conducted using Jade 6+(EasyQuant) software.

Wetting experiments were conducted in a static air box furnace fitted with a quartz door through which the heated specimen could be observed. A high-speed video camera equipped with a zoom lens was used to record the melting and wetting behavior of the glass (in pellet form) on a given substrate. Select frames from the videotape were converted to computer images, from which the wetting angle between the glass and substrate could be measured and correlated with the temperature log from the heating run. High-temperature viscosity measurements were conducted in a dynamic mechanical analyzer (DMA; DMA7e, PerkinElmer, Norwalk, CT). Glass tape specimens were heated between two 430 stainless steel disks at a rate of 1 °C min^{-1} to the soak temperature of interest, after which a static or dynamic load was applied to determine the material's viscoelastic response as a function of temperature.

Modulus of rupture (MOR) sample bars were prepared by laminating and firing a series of cast tapes at 1 °C min^{-1} to 850 °C for 1 h and cooling to room temperature at 3 °C min^{-1} to form a glass block. Two sets of glass blocks were made with one being heat-treated in static air at 750 °C for 4 h, while the other was held for 1000 h. After crystallization the glass blocks were ground flat and machined to a nominal dimension of 3 mm × 4 mm × 45 mm. To minimize sources of stress concentration, the edges were also rounded with SiC sand paper (#600). MOR tests were conducted using a SiC four-point bend test fixture fabricated with an outer span of 40 mm and an inner span of 20 mm. The tests were performed in air at both room temperature and 750 °C under a cross-head speed of 0.5 mm min^{-1}. For the 750 °C tests, the specimens were heated at 5 °C min^{-1} and allowed to equilibrate at temperature for 1/2 h prior to testing.

Table 2
Glass compositions (by mol%) that display high CTEs

Glass ID	BaO	CaO	Al_2O_3	B_2O_3	La_2O_3	CuO	SiO_2
18	35	15	5	10			35
21	35	10	5	15			30
23	32.5	12.5	2.5	12.5	5		35
24	32.5	12.5	2.5	10	3.5		39

3. Results and discussion

The thermal properties of the most promising compositions (out of 24 originally prepared) with respect to thermal expansion matching are listed in Table 2. The corresponding CTEs in the as-formed and as-crystallized conditions are given in Table 3. The average CTEs for the as-reduced anode and Crofer substrates are both ~12.5 × 10^{-6} K^{-1} [11]. All four formulations display CTEs that are acceptable for sealing the anode-supported cell and metallic separator components. Note that the glass transition temperature, T_g, is proportional to the ratio of B_2O_3 to SiO_2, which agrees with previously reported results on the thermal properties of borosilicate glasses [12]. As expected, the CTEs of these glasses increase with BaO and CaO content although, as will be discussed, the same trend does not occur for the crystallized product. Among the compositions listed, the G-18 glass displays the least thermal mismatch with the anode at temperatures below the glass transition temperature and therefore was chosen for more extensive testing. DMA measurements on this glass composition indicate that 850 °C is a near-optimal temperature for sealing. Above this temperature, the viscosity of the glass drops, eventually becoming too low to fabricate an adequate joint.

The CTE of the de-vitrified glass is dependent on the type and amount of crystalline phases that form in the material. A plot of this for G-18 as a function of time held at 750 °C is shown in Fig. 2. The graph was constructed from a series of quantitative XRD measurements conducted on the aged glass–ceramic

Table 3
Thermal properties of the compositions in Table 2

Glass ID	T_g (°C)	T_s (°C)	CTE, glass (×10^{-6} °C^{-1}; 25 °C–T_g)	CTE, crystallized (×10^{-6} °C^{-1}; 25 °C–1000 °C)	SiO_2/B_2O_3
18	630	685	11.8	10.8	3.5
21	575	628	11.2	12.5	2.0
23	628	662	11.4	12.1	2.8
24	633	665	11.5	12.2	3.9

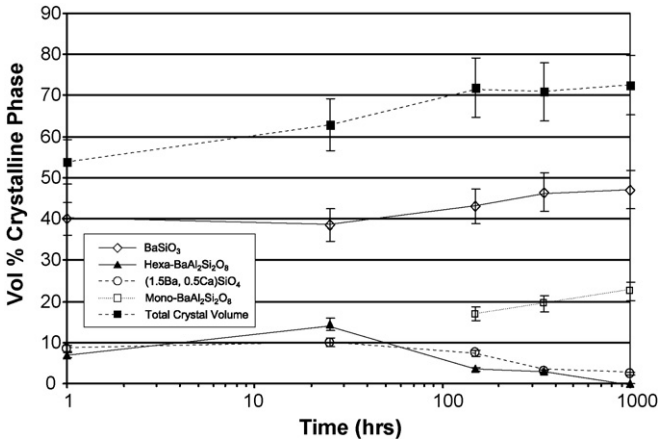

Fig. 2. Quantity of crystalline phases formed in G-18 as a function of time held in air at 750 °C.

samples. Note for example that just after sealing at 850 °C the glass has devitrified by ~50% on a volumetric basis. The dominant crystalline phases in the material at this point are barium silicate ($BaSiO_3$), barium calcium orthosilicate ($Ba_3CaSi_2O_8$), and hexacelsian ($BaAl_2Si_2O_8$). As has been previously described by Weinberg [25], the degree of crystallization is also dependent on the starting frit particle size (typically more rapid rates of devitrification are measured with reduced particle size), which is related to surface crystallization effects. Similar results have been observed with the G-18 glass and will be the subject of an upcoming article.

Under isothermal heating, the glass continues to crystallize up to an aging period of ~120 h, at which point the crystalline make-up of the glass–ceramic levels off to ~70 vol%. However as seen in the sequence of micrographs in Fig. 3, continued high-temperature aging does lead to additional crystallization as well as microstructural evolution in the material, albeit at a slower rate than observed in the initial de-vitrification process. Throughout aging, barium silicate remains the primary crystalline component. In fact, the relative amount of this phase slowly increases with time held at temperature. At ~60 h, the metastable hexacelsian constituent begins to transform to the more stable monoclinic structure. It is the formation of this phase that causes the significant decrease in CTE observed for the thermally aged bulk glass–ceramic.

Listed in Table 4 are the average CTEs of the crystalline phases found in de-vitrified G-18. Monocelsian by far exhibits the lowest CTE of the group. The net effect is a reduction in the CTE of the glass–ceramic with continuous high-temperature exposure, as illustrated in Fig. 4. Upon joining at 850 °C, the CTE of the bulk glass–ceramic nearly matches that of the reduced bilayer substrate. However after 1 week of exposure, enough monocelsian has formed to drop the composite CTE by 15%. The CTE increases slightly after

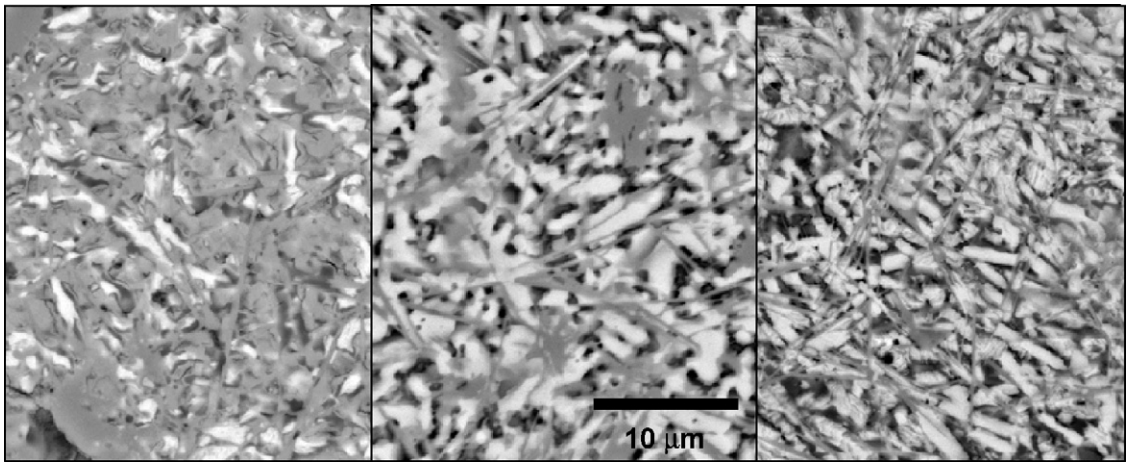

Fig. 3. SEM micrographs of G-18 after aging in 750 °C air for: (a) 50 h, (b) 730 h, and (c) 1200 h. The de-vitrified glass is composed of several crystalline phases, notably: $BaSiO_3$ (oblate white crystals), $BaAl_2Si_2O_8$ (needle-shaped dark gray crystals), and $Ba_3CaSi_2O_8$ (large, blocky gray crystals).

Table 4
CTEs for crystalline phases in de-vitrified G-18

Phase	Composition	CTE ($\times 10^{-6}$ °C^{-1})	T range (°C)	Ref.
Quartz	SiO_2	11.2	20–100	[14]
		13.2	20–300	
		23.3	20–600	
Enstatite	$MgSiO_3$	9	20–400	[14]
		12	300–700	
Clinoenstatite	$MgSiO_3$	7.8	100–200	[14]
		13.5	300–700	
Protoenstatite	$MgSiO_3$	9.8	300–700	[14]
Forsterite	Mg_2SiO_4	9.4	100–200	[14]
Wollastonite	$CaSiO_3$	9.4	100–200	[14]
Calcium orthosilicate	Ca_2SiO_4	10.8–14.4	100–200	[14]
Barium silicate	$BaSiO_3$	~12.5	20–550	Measured at PNNL
		~10.5	20–1000	Measured at PNNL
Hexacelsian[a]	$BaAl_2Si_2O_8$	~8	20–1000	[15]
Monocelsian	$BaAl_2Si_2O_8$	~2.3	20–1000	[15]

[a] Metastable at <1590 °C

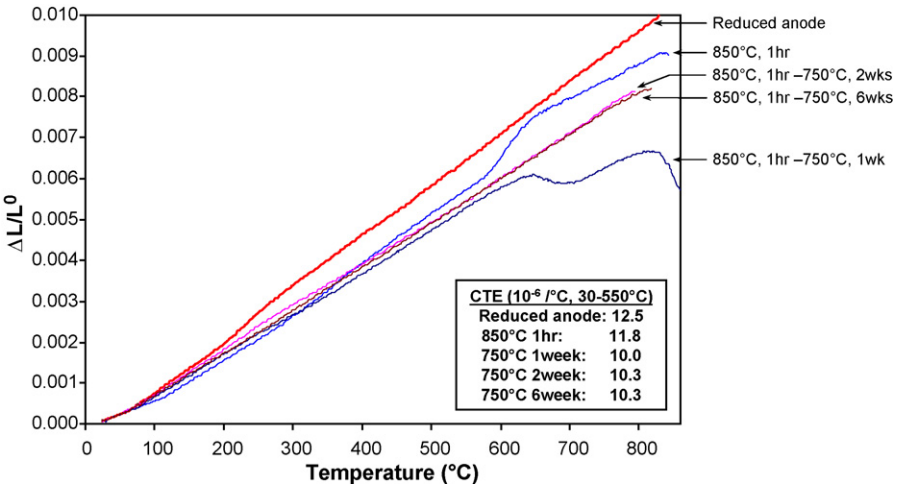

Fig. 4. Thermal expansion of G-18 as a function of temperature after thermal aging in air at 750 °C.

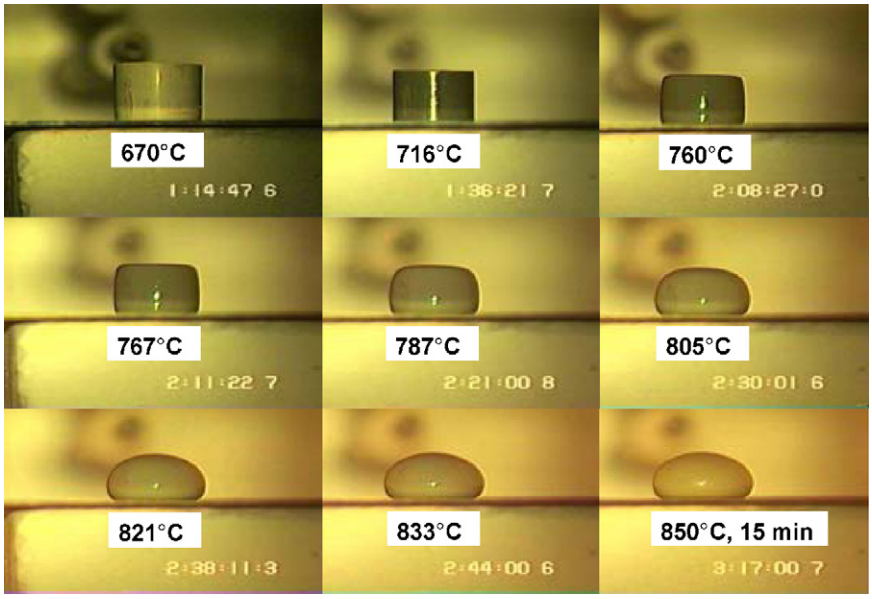

Fig. 5. A sequence of photographs of a G-18 pellet as it is heated to the temperature typically used in joining.

2 weeks of exposure with additional formation of $BaSiO_3$, and then stabilizes as the rate of devitrification slows to nearly zero. As mentioned previously, at pSOFC operating temperatures most glasses will crystallize with time. Therefore, it is critical that the glass composition not only display good initial CTE matching with the adjoining substrates, but also that the CTE remains relatively constant as the material de-vitrifies. Once fully crystallized, the resulting glass–ceramic tends to be very stable over long periods of time at high temperature.

The wetting characteristics of the G-18 glass were examined by monitoring the change in shape of a pellet specimen on various substrates. A representative example of this is shown in Fig. 5. Note that at the sealing temperature, the contact angle is greater than 90°, i.e., non-wetting. Thus pressure is required to facilitate adequate joining when using the glass at this temperature. In order to achieve a wetting angle less than 90°, the glass must be heated to temperatures in excess of 1000 °C. However as shown in Fig. 6, the DMA data indicate that the viscosity is too low to ensure reliable sealing. That is, the glass tends to flow excessively during joining, causing gaps (and subsequently leaks) to form within the seal. A

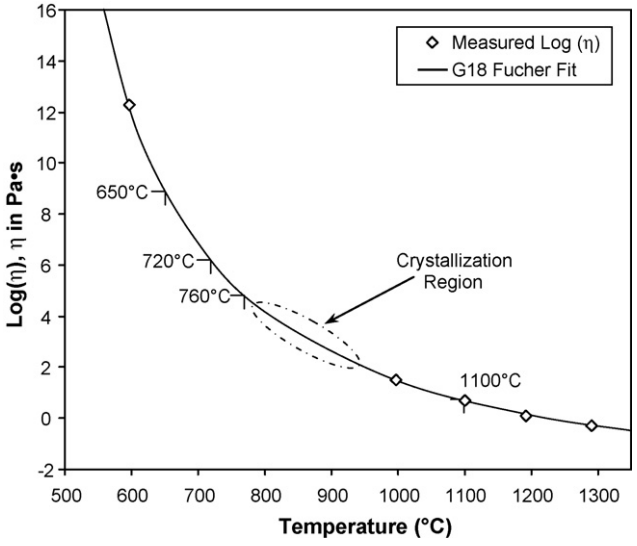

Fig. 6. The viscosity of G-18 plotted logarithmically as a function of temperature.

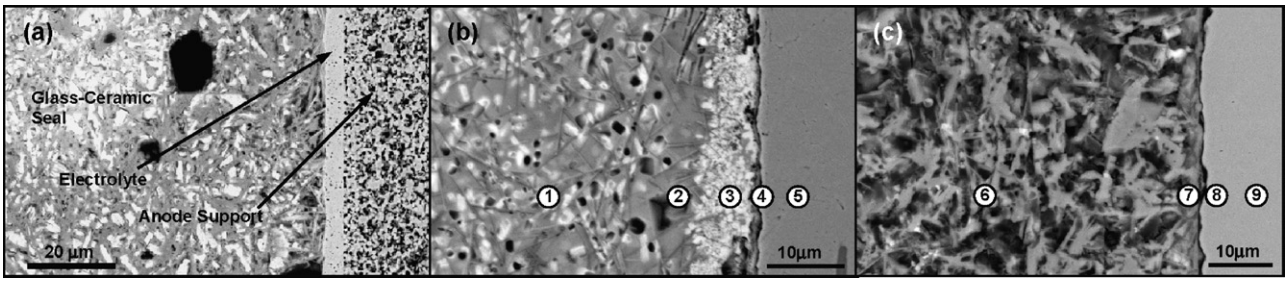

Fig. 7. SEM micrographs of G-18 in contact with: (a) 5YSZ after aging in 750 °C air for 1200 h, (b) 446 in the as-joined condition, and (c) FeCrAlY in the as-joined condition.

trend line can be fitted to the viscosity data using the empirical Vogel–Fulcher relation [26]:

$$\eta = E \exp\left[\frac{F}{T - T_o}\right] \quad (1)$$

where E and F are curve fitting constants and T_o is a threshold temperature in the vicinity of the glass transition temperature T_g. The expression is analogous to the Williams–Landel–Ferry equation derived from free-volume theory for viscous liquid flow, which assumes that the critical step in flow is the opening or formation of a critical volume of void space that permits a sufficient level of molecular motion within the material [26].

As shown in Fig. 7(a), the G-18 glass exhibits little interaction with the 8YSZ substrate after 1200 h in 750 °C air. A very small amount of $BaZrO_3$ forms at the interface between the glass and 8YSZ, which if it remains sub-micron in thickness throughout the lifetime of the device may enhance the bonding along this interface. On the other hand, as shown in Fig. 7(b) and (c) a more substantial reaction zone forms between the glass and two different respective interconnect alloys in the as-joined condition (850 °C, 4 h). Corresponding chemical analysis for each of the regions labeled in the two figures are listed in Table 5. In the case of the chromia-scale forming steel, 446, five microstructurally distinct zones can be readily observed in the micrograph of the G-18/446 joint shown in Fig. 7(b): (1) the devitrified glass–ceramic in the bulk portion of the seal, (2) an adjacent glass–ceramic region that is measurably depleted in barium (and therefore appears to be composed predominantly of aluminosilicate), (3) a ~10-μm thick reaction zone between the chromia scale and the glass, (4) a chromia scale that forms on the surface of the alloy during joining, and (5) the bulk 446 stainless steel. EDX analysis conducted on Region (3) indicates that the primary phase in the interfacial reaction zone is $BaCrO_4$. These findings are similar to those reported previously by Yang et al. [21,22] From oxidation studies conducted on 446, the parabolic rate constant associated with chromia growth on the alloy is 3.43×10^{-14} cm^2 s^{-1} at 850 °C [11]. Using Wagner's equation [27] for the rate of protective scale growth, one can estimate the maximum thickness of chromia expected to form on the 446 during joining, $t_{4\,h,\,850\,°C} \sim 0.1$ μm. The chromia scale appears to react directly with baria in the glass to form the chromate product. This is consistent with the depletion of barium and lack of chromium observed in the material of Region (2) and corresponds with previous observations reported between BAS-based glasses and chromia-forming steels [21].

In contrast, the FeCrAlY forms a much thinner oxide scale during sealing, in this case composed primarily of alumina, and subsequently exhibits a much thinner reaction zone between the bulk glass and the scale. At 5.13×10^{-16} cm^2 s^{-1} [11], the oxidation rate of FeCrAlY at 850 °C is almost two orders of magnitude lower than that of 446. Thus, when exposed to 850 °C air during the sealing step, the alloy will develop a scale that is less than 0.01 μm thick. From the EDX analysis, the composition of the interfacial reaction zone corresponds to celsian, or $BaAl_2Si_2O_8$, in either the hexagonal or monoclinic structure. Although monocelsian is thermodynamically the more stable phase, hexacelsian typically forms preferentially

Table 5
EDX results for points marked in Fig. 7(b) and (c)

Element	Composition (at%)						
	O	Al	Si	Ca	Cr	Fe	Ba
Pt 1	57.4	3.8	18.2	2.6	–	–	18.0
Pt 2	55.9	19.2	19.6	1.9	–	–	3.4
Pt 3	65.1	1.9	4.2	0.6	13.3	0.2	14.7
Pt 4	57.8	0.8	1.9	1.0	35.9	0.6	2.0
Pt 5	–	–	–	–	23.3	76.3	–
Pt 6	55.9	5.4	19.6	1.3	–	–	17.8
Pt 7	59.0	14.8	16.3	1.3	1.7	0.3	6.6
Pt 8	52.9	36.8	0.1	–	6.7	3.5	–
Pt 9	–	4.3	0.5	–	21.6	73.6	–

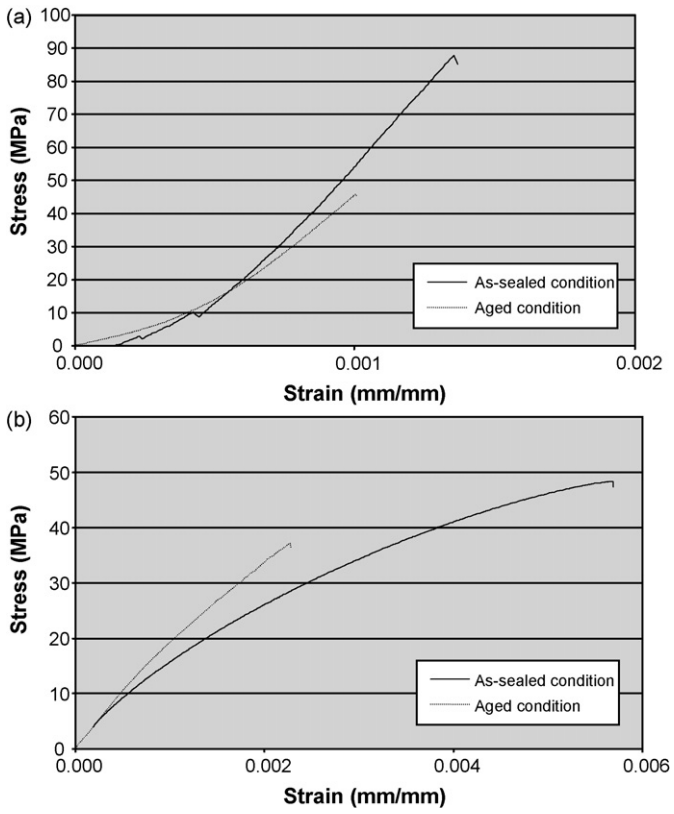

Fig. 8. Stress–strain curves for the bulk G-18 sealant, as determined from flexural testing conducted at: (a) room temperature and (b) 750 °C. Plotted in each figure are curves for the material in the "as-sealed" condition (after 4 h at 850 °C) and after aging the as-sealed material for 1000 h at 750 °C.

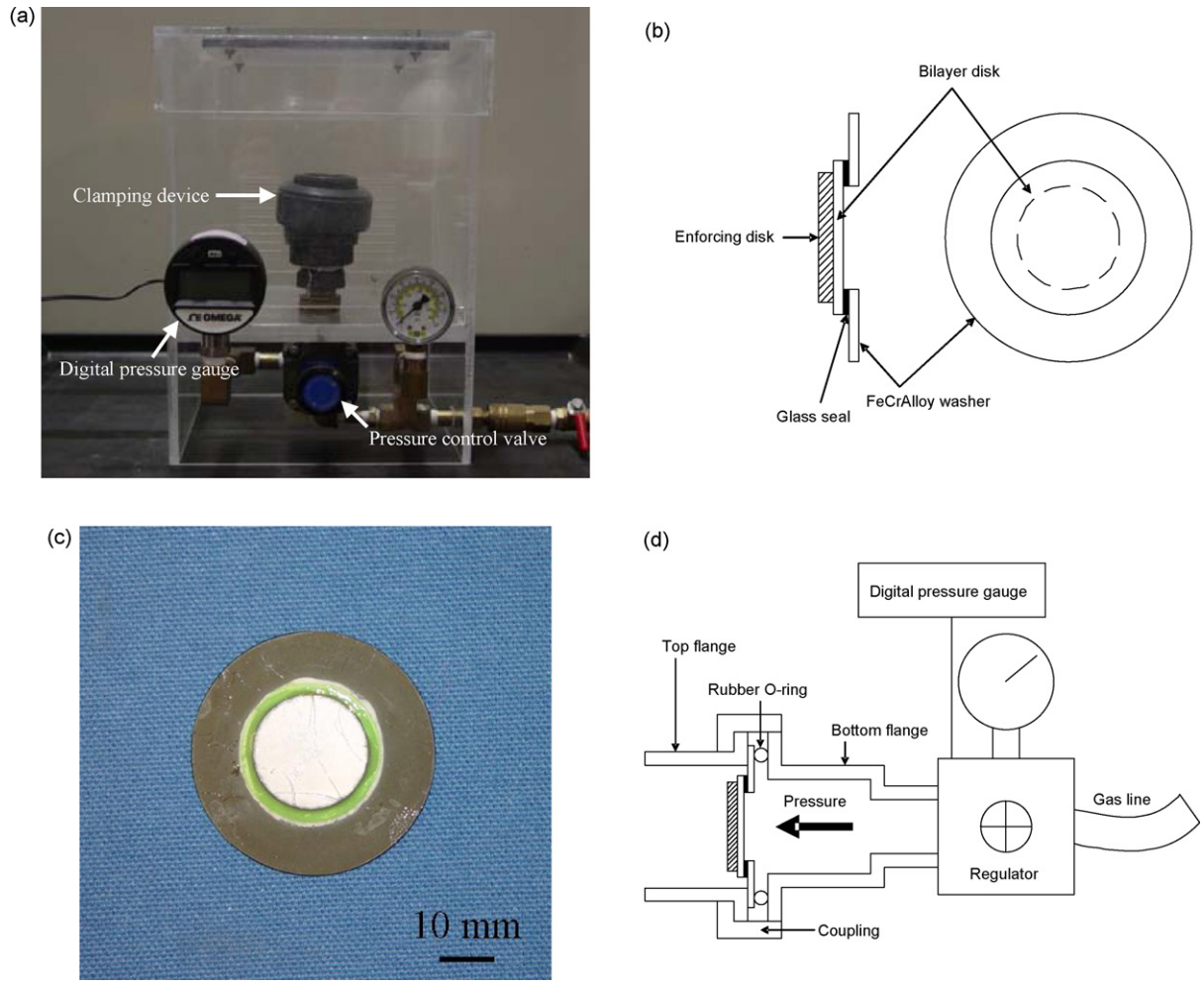

Fig. 9. A simple test fixture [29] designed to quantitatively evaluate the strength of the glass seal joint: (a) a photograph of the test fixture, which is composed of a digital pressure gage, a clamping device, and a pressure control valve that is connected to the pressurized air (or inert gas); (b) a schematic of the specimen designed for rupture testing, (c) an example of a prepared rupture test specimen, and (d) a schematic of a specimen undergoing testing.

due to more favorable reaction kinetics [28]. We assume this is the case here, at least in the as-joined condition. Thus in cross-section, the joining sample in Fig. 7(c) consists of four microstructurally distinct regions: (1) the bulk alloy, (2) a very thin alumina scale, (3) a ~1-μm thick celsian reaction zone, and (4) the bulk devitrified glass.

The stress/strain behaviors of the bulk G-18 glass at room temperature and 750 °C are shown respectively in Fig. 8(a) and (b). Plotted in each graph are data for the bulk G-18 material in the nascent condition (i.e., aged under a simulated bonding heat treatment of 4 h in ambient air at 850 °C) and after aging in air at 750 °C for 1000 h beyond the nascent as-joined condition. As seen in Fig. 8(a), the two samples tested at room temperature display typical brittle behavior, with elastic failure occurring at maximum load/stress. The two small kinks in the data recorded for the nascent specimen were likely due to a small amount of slippage between the test fixture and specimen. The nascent sample exhibits higher strength than the aged sample, ~85 MPa versus ~45 MPa, respectively. Although devitrification can sometimes lead to strengthening in glass–ceramics, more often crystallization causes weakening at least at temperatures below T_g. This is because as crystalline phases precipitate out of the homogeneous parent glass, the resulting inhomogeneities in mechanical properties such as elasticity and CTE generate localized regions of residual stresses throughout the material that serve as defect sites for crack initiation and brittle failure. Accordingly, the correlation between the final devitrified microstructure and mechanical properties is strongly dependent on, among other factors, the amount of residual glass in the composite material and its corresponding viscosity (or mechanical response) during the devitrification event. That is, much of the localized residual stress can be accommodated if the viscosity of the glassy matrix is low or if sufficient time (i.e., annealing) is allowed for plastic flow.

The latter process is likely the reason why the difference in strength between the nascent and aged materials is relatively small at a test temperature of 750 °C, ~48 MPa versus 38 MPa, respectively. Note that both of the samples tested at high temperature still exhibit brittle failure, even though each exhibits non-linear elastic behavior (i.e., the slope of the σ–ε curve not constant with strain), which is particularly apparent in the case of the nascent specimen. The greater strain at fracture in the nascent material relative to aged material is due to the larger amount of residual glass present in the former and to the entanglement (or close proximity) of the crystalline phases in the latter. The entanglement of crystalline phases in the aged specimen also explains the greater amount of strength retention found when contrasting the results of room temperature and 750 °C testing for this material. By comparison, the nascent material displays far less strength retention, exhibiting a 43% drop in strength from room temperature to 750 °C.

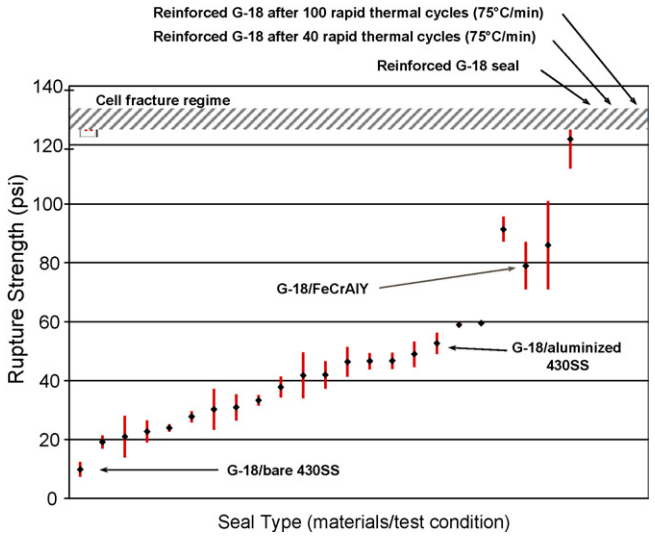

Fig. 10. Progressive improvements in rupture strength results. The maximum pressure of the test device is 130 psi.

Independent of chemical composition, there are a number of other factors that can play a significant role in the performance characteristics of a given sealant such as G-18, including: the particle size of the original glass powder frit; the ratio of glass frit and binder in paste and tape casting formulations; the composition, thermal expansion, and oxidation properties of the substrates being joined, in particular metal substrates; the initial joining heat treatment conditions; and the subsequent transient and steady state operational conditions (e.g., heating and cooling rates and accumulative number of thermal cycles). To screen the vast number of material, processing, and operational parameters involved in glass sealing, we have developed a simple semi-quantitative mechanical test known as the rupture test. A schematic of the test apparatus is shown in Fig. 9. Essentially a modified version of an adhesive blister testing technique [29], the test is conducted by placing a sealed disk specimen in a test fixture and slowly pressurizing the backside of the sample until seal rupture occurs, which gives a measure of the maximum pressure that the specimen can withstand. That is, the specimen is subjected to an accelerated stress test, using air pressure to generate high levels of stress within the seal. A maximum pressure of 130 psi and a minimum of six specimens for each joining condition were employed in testing.

As shown in Fig. 10, rupture test specimens fabricated with an alternative chromia-forming ferritic alloy, 430 stainless steel, exhibit a low average rupture strength of ~8 psi. The low strength is likely due to the thick barium chromate product that forms between the glass matrix and the chromia scale on the 430. Additional investigation is needed to determine this more precisely. Regardless, independent thermomechanical modeling [30] of a full-scale stack suggests that this level of strength is too low to survive the type of aggressive thermal cycling conditions anticipated in a number of power generation devicess; e.g., pSOFC auxiliary power units (APUs) being developed for use in various transportation and military applications. [31]. The use of aluminized 430 (i.e. which exhibits an oxidation-resistant alumina scale surface) shows a fourfold increase in rupture strength, within range for potential use in a truck or automotive APU. As an indication of further progress with this joining technology, additional improvements were achieved by reinforcing the sealant [32]. A series of rupture test specimens prepared with the reinforced seal were subsequently exposure tested as follows: 1000 h soak at 750 °C, 10 rapid thermal cycles from below 200 °C to 750 °C at a rate of 75 °C min^{-1}, then followed by a 500-h soak at 750 °C. None of the samples displayed leaking after exposure testing and all could be pressurized to the maximum pressure of the test apparatus without failure.

4. Conclusions

The thermal properties, chemical stability, bonding characteristics, and mechanical strength of a series of BAS-based glasses have been investigated to develop a sealing glass composition that is suitable for use in a moderate temperature pSOFC. The results indicate the following:

- One specific composition (G-18; 35 BaO, 15 CaO, 10 B_2O_3, 5 Al_2O_3, and bal. SiO_2) was found to exhibit particularly good CTE stability as a function of time at 750 °C.
- DMA indicates that the viscosity of G-18 is optimal with respect to sealing at 850 °C; i.e., a good balance is achieved between glass softening and the rate of crystallization, affording good sealant deformation, substrate wetting, and gap filling when seals are produced at this temperature under a modest load. The primary crystallization product is barium silicate ($BaSiO_3$).
- A small decline in CTE is observed in the G-18 material as a function of aging at 750 °C due to the transformation of one of the crystalline product phases, hexacelsian, to its more thermodynamically stable monoclinic crystal structure.
- Wetting studies indicate that the contact angle of the G-18 composition is greater than 90° (i.e., non-wetting) at 750 °C, but does decrease below 90° at temperatures above ~1000 °C. Thus to carry out bonding/sealing at 750 °C, the joint must be compressively loaded.
- Flexural testing of the bulk sealant indicates that there is a drop in the strength of the material upon devitrification, although the difference in strength between the nascent and devitrified glasses is more significant at room temperature than at projected operating temperature. Additionally, modeling estimates of sealant stresses/strains in the APU application suggest that the bulk strength of G-18 in the aged condition will be acceptable for both transient and steady-state operating conditions.
- Of greater concern is the interfacial strength between the sealant and the metallic components, which is dependent on the extent of interaction between the two materials as a function of time at temperature under the variable gas atmosphere (e.g., gradients in water content from air inlet to air outlet). This issue has been one of the drivers for our latest research and development work.
- The glass–ceramic resulting from glass sealing with the G-18 composition displays little interaction with the YSZ electrolyte layer on the cell. However, a reaction zone does develop between the sealant and the in situ formed oxide scales of both chromia- and alumina-forming stainless steels. To a certain extent this is useful, as long as the reaction product is mechanically strong and reasonably thin. While this is the case with the alumina-fomers, it is not with the chromia scale forming alloys. Subsequent joint strength testing indicates a fourfold difference in strength between the two stainless steel materials.

Acknowledgements

The authors would like to thank Nat Saenz, Shelly Carlson, and Jim Coleman for their assistance in preparing the metallographic samples. This work was supported by the U.S. Department of Energy, Office of Fossil Energy, Advanced Research and Technology Development Program. The Pacific Northwest National Laboratory is operated by Battelle Memorial Institute for the United States Department of Energy (U.S. DOE) under Contract DE-AC06-76RLO 1830.

References

[1] B.C.H. Steele, A. Heinzel, Nature 414 (2001) 345.
[2] S.-B. Sohn, S.-Y. Choi, G.-H. Kim, H.-S. Song, G.-D. Kim, J. Am. Ceram. Soc. 87 (2004) 254.
[3] P.H. Larsen, C. Bagger, M. Mogensen, J.G. Larsen, Proceedings of the Fourth International Symposium on Solid Oxide Fuel Cells, vol. 95-1, The Electrochemical Society, 1995, p. 69.
[4] C. Günther, G. Hofer, W. Kleinlein, Proceedings of the Fifth International Symposium on Solid Oxide Fuel Cells, vol. 97-18, The Electrochemical Society, 1997, p. 746.
[5] K.L. Ley, M. Krumpelt, R. Kumar, J.H. Meiser, I. Bloom, J. Mater. Res. 11 (1996) 1489.
[6] Y. Sakaki, M. Hattori, Y. Esaki, S. Ohara, T. Fukui, K. Kodera, Y. Kubo, Proceedings of the Fifth International Symposium on Solid Oxide Fuel Cells, vol. 97-18, The Electrochemical Society, 1997, p. 652.
[7] C.-K. Lin, T.-T. Chen, Y.-P. Chyou, L.-K. Chiang, J. Power Sources 164 (2007) 238.
[8] S. Taniguchi, M. Kadowaki, T. Yasuo, Y. Akiyama, Y. Miyake, K. Nishio, J. Power Sources 90 (2000) 163.
[9] S.P. Simner, J.W. Stevenson, J. Power Sources 102 (2001) 310.
[10] K.P. Recknagle, R.E. Williford, L.A. Chick, D.R. Rector, M.A. Khaleel, J. Power Sources 113 (2003) 109.
[11] Z. Yang, K.S. Weil, D.M. Paxton, J.W. Stevenson, J. Electrochem. Soc. 150 (2003) A1188.
[12] P.H. Larsen, F.W. Poulsen, R.W. Berg, J. Non-Cryst. Solids 244 (1999) 16.
[13] K. Eichler, G. Solow, P. Otschik, W. Schaffrath, J. Eur. Ceram. Soc. 19 (1999) 1101.
[14] I.W. Donald, J. Mater. Sci. 28 (1993) 2841.
[15] N.P. Bansal, M.J. Hyatt, J. Mater. Res. 4 (1989) 1257.
[16] C. Lara, M.J. Pascual, A. Duran, J. Non-Cryst. Solids 348 (2004) 149.
[17] J.-H. Piao, K.-N. Sun, N.-Q. Zhang, D.-R. Zhou, J. Hua, J. Synth. Cryst. 33 (2004) 909.
[18] S. Ohara, K. Mukai, T. Fukui, Y. Sakaki, M. Hattori, Y. Esaki, J. Ceram. Soc. Jap. 109 (2001) 186.
[19] K. Ogasawara, H. Kameda, Y. Matsuzaki, T. Sakurai, T. Uehara, A. Toji, N. Sakai, K. Yamaji, T. Horita, H. Yokokawa, J. Electrochem. Soc. 154 (2007) B657.
[20] S.-M. Gross, T. Koppitz, J. Remmel, U. Reisgen, Ceram. Eng. Sci. Proc. 26 (2005) 239.
[21] Z. Yang, K.D. Meinhardt, J.W. Stevenson, J. Electrochem. Soc. 150 (2003) A1095.
[22] Z. Yang, G. Xia, K.D. Meinhardt, K.S. Weil, J.W. Stevenson, J. Mater. Eng. Perform. 13 (2004) 327.
[23] S. Mukerjee, K. Haltiner, S. Shaffer, K.D. Meinhardt, L.A. Chick, V. Sprenkle, S. Weil, J.Y. Kim, Proceedings of the Electrochemical Society, SOFC IX, PV 2005-07, 2005, p. 48.
[24] K.S. Weil, JOM 58 (2006) 37.
[25] M.C. Weinberg, J. Non-Cryst. Solids 255 (1999) 1.
[26] W.D. Kingery, H.K. Bowen, D.R. Uhlmann, Introduction to Ceramics, 2nd ed., John Wiley & Sons, 1976, p. 759.
[27] C. Wagner, Atom Movements, American Society of Metals, Cleveland, OH, 1951.
[28] Y.-M. Sung, J. Mater. Sci. Lett. 19 (2000) 453.
[29] K.S. Weil, J.E. Deibler, J.S. Hardy, D.S. Kim, G.-G. Xia, L.A. Chick, C.A. Coyle, J. Mater. Eng. Perform. 13 (2004) 316.
[30] M. Lang, P. Szabo, Z. Ilhan, S. Cinque, T. Franco, G. Schiller, J. Fuel Cell Sci. Technol. 4 (2007) 384.
[31] P. Lamp, J. Tachtler, O. Finkenwirth, S. Mukerjee, Shaffer, Fuel Cells 3 (2003) 146.
[32] K.S. Weil, L.A. Chick, C.A. Coyle, J.S. Hardy, G. Xia, K.D. Meinhardt, V.L. Sprenkle, D.M. Paxton, European Patent EP 1836138, issued 9/26/07.